Electrochimica Acta 165 (2015) 7–13

Contents lists available at ScienceDirect

Electrochimica Acta

journal homepage: www.elsevier.com/locate/electacta

# Nitrogen-Doped Carbon Nanodots@Nanospheres as An Efficient Electrocatalyst for Oxygen Reduction Reaction

Haimin Zhang [a,b,*], Jiangyao Chen [b,c], Yibing Li [b], Porun Liu [b], Yun Wang [b], Taicheng An [c], Huijun Zhao [a,b,*]

[a] Centre for Environmental and Energy Nanomaterials, Institute of Solid State Physics, Chinese Academy of Sciences, Hefei 230031, China
[b] Centre for Clean Environment and Energy, Griffith University, Gold Coast Campus, QLD 4222, Australia
[c] State Key Laboratory of Organic Geochemistry, Guangzhou Institute of Geochemistry, Chinese Academy of Sciences, Guangzhou 510640, China

ARTICLE INFO

*Article history:*
Received 27 October 2014
Received in revised form 15 January 2015
Accepted 28 February 2015
Available online 3 March 2015

*Keywords:*
Nitrogen-doped carbon nanodots
Microporous carbon nanospheres
Natural biomass
Electrocatalyst
Oxygen reduction reaction

ABSTRACT

In this work, nitrogen-doped carbon nanodots (N-CNDs) with sizes of 2–6 nm were successfully synthesized by hydrothermal treatment of natural biomass (*e.g.*, fresh grass) at 180 °C for 10 h. The synthesized carbon nanodots were subsequently immobilized onto functionalized microporous carbon nanospheres (MCNSs) with an average diameter of ~100 nm and a surface area of 241 $m^2 g^{-1}$ *via* a simple hydrothermal process to self-assembly form a carbon-based nanocomposite (N-CNDs@MCNSs) owing to the presence of oxygen (O)-containing surface functional groups. As electrocatalyst for oxygen reduction reaction (ORR) application, our experimental results demonstrated that sole N-CNDs could not form stable electrocatalyst film for ORR measurement owing to their high water dispersion property, while the N-CNDs@MCNSs exhibited high electrocatalytic activity with an onset potential of −0.08 V, superior durability and high resistance to methanol cross-over effect, comparable to commercially available Pt/C electrocatalyst.



## 1. Introduction

Owing to the unique physical and chemical properties, carbon-based nanomaterials (*e.g.*, nanotubes, nanosheets, nanospheres and nanodots) have been extensively investigated for optoelectronic devices, energy storage applications, electrocatalysis, photocatalysis, and environmental applications [1–10]. The reported findings have demonstrated that the performance of such carbon-based materials could be significantly improved by further functionalizations [11–14]. Recently, heteroatom (*e.g.*, N, B, S, P) doped carbon-based nanomaterials have demonstrated to be a class of promising metal-free electrocatalysts for oxygen reduction reaction (ORR) to replace Pt-based electrocatalysts with inherent disadvantages of high cost, resource scarcity and low tolerance to fuel molecules (*e.g.*, methanol) [4,15–23]. However, development of more efficient, cheaper and earth-abundant metal-free ORR electrocatalysts is highly challenging and critically important for large-scale practical use of the fuel cell technology.

Very recently, nitrogen-doped carbon nanodots (N-CNDs), nitrogen-doped graphene quantum dots (N-GQDs) and their corresponding composites (*e.g.*, CuS/CNDs, Ag/CNDs) synthesized by various methods have successfully demonstrated great potential as superior ORR electrocatalysts [15,22–26]. However, the reported results indicate that an ORR electrode prepared by directly coating N-CNDs or N-GQDs electrocatalyst onto glassy carbon (GC) electrode is often suffered from poor uniformity and stability due to their high water dispersion property and easy aggregation nature [23,24]. In this respect, our and other groups have tried to immobilize N-CNDs (or N-GQDs) onto conductive carbon nanosheets (or graphene nanosheets) *via* simple treatment approaches to form carbon-based nanocomposites [23,24]. The resulting carbon materials as electrocatalysts can form stable and uniform catalyst films onto GC electrodes, avoiding catalyst falling off and displaying superior ORR catalytic activity [23,24]. Owing to easy synthesis, cheap reaction sources and superior ORR catalytic activity of N-CNDs and N-GQDs, it is of great significance to explore more approaches to fabricate N-CNDs (or N-GQDs) based metal-free electrocatalysts for ORR application in a simple, economic, efficient and environmentally friendly manner.

Herein, we report a new approach to obtain stable carbon-based electrocatalyst with superior electrocatalytic activity. The microporous carbon nanospheres (MCNSs) with diameters of

* Corresponding authors. Tel: +86 551-65591263; fax: +86 551-65591434.
*E-mail addresses:* zhanghm@issp.ac.cn (H. Zhang), h.zhao@griffith.edu.au (H. Zhao).

http://dx.doi.org/10.1016/j.electacta.2015.02.240
0013-4686/

~100 nm were firstly synthesized by a reported hydrothermal process [27] and further treated by acidification approach to obtain surface functionalization (see experimental section). Nitrogen-doped carbon nanodots (N-CNDs) coated MCNSs (N-CNDs@MCNSs) were fabricated by simple hydrothermal treatment of a suspension solution containing N-CNDs and acidification treated MCNSs at 180 °C for 5 h. As ORR electrocatalyst, the resultant N-CNDs@MCNSs can form stable and uniform catalyst film onto glassy carbon (GC) electrode, displaying superior ORR electrocatalytic activity with high durability, comparable to commercial Pt/C electrocatalyst.

## 2. Experimental

### 2.1. Preparation of MCNSs, N-CNDs and N-CNDs@MCNSs

Microporous carbon nanospheres (MCNSs) were synthesized using a simple hydrothermal process, as reported by Fang et al. [27]. In a typical synthesis, low molecular weight phenolic resol was firstly prepared by stirring a mixed solution containing 0.6 g phenol, 2.1 mL of formalin solution (37 wt%) and 15 mL of 0.1 M NaOH solution at 70 °C for 30 min. Subsequently, 0.96 g triblock copolymer Pluronic F127 (Mw = 12600) was dissolved in 15 mL of Milli-Q water, and then added slowly to the above low molecular weight phenolic resol solution. The mixture was subsequently stirred at 65 °C for 2 h, and then 50 mL of water was added to dilute the above solution. After 17 h, 17.7 mL of the above solution was further diluted using 56 mL of water, and the mixture was then transferred into an autoclave to perform a hydrothermal reaction at 130 °C for 24 h. After hydrothermal reaction, the product was collected by centrifugation and washed adequately with Milli-Q water. Finally, MCNSs was obtained by high temperature carbonization of the room temperature dried product at 700 °C in $N_2$ atmosphere for 3 h. For further functionalization, the obtained MCNSs were treated ultrasonically in a mixed solution of concentrated $H_2SO_4$ and $HNO_3$ with a volume ratio of 3:1. After 30 min, the product was collected by centrifugation and then rinsed adequately by water, finally dried in room temperature for a further characterization and use.

N-doped carbon nanodots (N-CNDs) were synthesized using previously reported methods [24,28,29]. In a typical synthesis, 20 g fresh Monkey Grass (*Ophiopogon Japonicus*) was firstly cut into pieces and added into 60 mL of deionized water (Millipore Corp., 18 MΩ), and then the mixture was transferred into a 100 mL of Teflon lined autoclave. The hydrothermal reaction was kept at 180 °C for 10 h. After hydrothermal reaction, the obtained product was collected by filtration (0.2 μm cellulose membrane) and centrifugation at 4500 rpm and 14,000 rpm for 10 min, respectively. The obtained nanodot solution was stored for further characterization and use. In this work, the fabricated N-doped carbon nanodot solution possesses a concentration of *ca.* 18 mg $mL^{-1}$ with a production yield of around 5.4%.

N-CNDs@MCNSs nanocomposite was synthesized by hydrothermal treatment of 20 mL of N-CNDs solution containing 0.5 g functionalized MCNSs at 180 °C for 5 h. The as-synthesized carbon nanospheres without functionalization are very hydrophobic that cannot be dispersed in water (photo (1), Scheme 1). An acidification treatment (Scheme 1) can readily transform the hydrophobic MCNSs into hydrophilic ones that are highly dispersible in water (photo (2), Scheme 1). N-CNDs with sizes of 2–6 nm (TEM image (3) and photo (4), Scheme 1) were then immobilized onto the synthesized hydrophilic MCNSs *via* simple hydrothermal treatment of a suspension solution containing N-CNDs and MCNSs at 180 °C for 5 h to obtain N-CNDs coated MCNSs (N-CNDs@MCNSs). The hydrothermal treatment leads to a change in the N-CNDs solution colour from brownish to light yellow (photos (4) and (5), Scheme 1), implying the N-CNDs could be loaded onto the MCNSs. After that, the product was collected by centrifugation and then washed adequately with water. After dried in room temperature, the loading amount of N-CNDs on MCNSs is about 0.6 mg $mg^{-1}$.

### 2.2. Characterizations

The morphologies of MCNSs and N-CNDs were characterized by scanning electronic microscopy (SEM, JSM 7001F) and transmission electronic microscopy (TEM, Philips F20), respectively. FT-IR spectra of the samples were measured to investigate structural information and specific molecule-groups information (Perkin-Elmer 2000). Chemical compositions of the samples were analyzed by X-ray photoelectron spectroscopy (XPS, Kratos Axis ULTRA incorporating a 165 mm hemispherical electron energy analyser). N-doped carbon nanodot loading amount onto microporous carbon nanospheres was measured by carefully calculating the weight of microporous carbon nanospheres before and after hydrothermal reaction. The Brunauer–Emmett–Teller method was utilized to calculate the specific surface area of N-CNDs@MCNSs sample using nitrogen adsorption–desorption isotherm on a Quantachrome Autosorb-1 equipment [30].

### 2.3. Measurements

All electrochemical measurements were performed using a three-electrode system (Pine Instrument, USA) consisting of a working electrode, an Ag/AgCl reference electrode (3.0 M) and a platinum mesh counter electrode. CV measurements were carried out using a computer-controlled potentiostat (CHI 760D, CH Instruments, USA) in a standard three-electrode cell at a scan rate

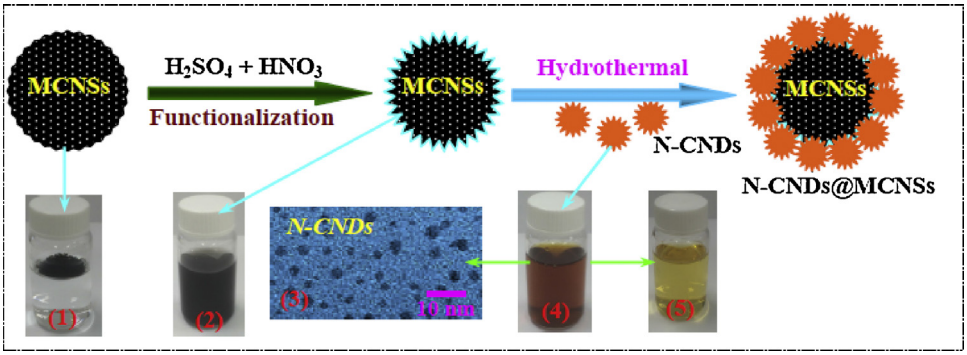


**Scheme 1.** Schematic illustration of a fabrication process of N-CNDs@MCNSs. (1) As-synthesized MCNSs in water; (2) Functionalized MCNSs in water; (3) TEM image of N-CNDs; (4) Original N-CNDs solution; (5) N-CNDs solution after hydrothermal reaction.

of 100 mV $s^{-1}$. Prior to measurements, RDE (GC, 5.0 mm in diameter, Pine Instrument) was firstly polished using 1.0, 0.3 and 0.05 μm alumina slurry sequentially, and then rinsed adequately using deionized water and ethanol in ultrasonic bath. The cleaned RDE was then dried in a $N_2$ stream for further coating MCNSs, N-CNDs@MCNSs, and commercial Pt/C (Vulcan, 20 wt.%) catalysts. 1.2 mg $mL^{-1}$ MCNSs, N-CNDs@MCNSs, and Pt/C solutions (in 0.5% Nafion aqueous solutions) were firstly prepared. 12 μL of the prepared catalyst solution was cast on the cleaned RDE, and then dried at 60 °C in air. The loading amount of catalyst on the RDE was *ca.*73 μg $cm^{-2}$. The catalyst coated glassy carbon electrode was placed in an electrochemical cell containing 60 mL of N-saturated or O-saturated 0.1 M KOH solution with or without 3 M methanol. All measurements were carried out using RDE (Pine Modulated Speed Rotator with CE Mark (Pine Instrument) controlled by a CHI 760D electrochemical potentiostat). Electrochemical impedance spectra (EIS) measurements of the catalysts were conducted using a symmetric two-electrode cell fabricated with two identical catalyst coated glassy carbon electrodes with a computer-controlled potentiostat (CHI 760D, CH Instruments, USA). The used electrolyte is $O_2$-saturated 0.1 M KOH solution. The measured frequency range is 0.1 Hz to 1 M Hz and the magnitude of the modulation signal is 10 mV.

### 2.4. Koutecky–Levich (K–L) Equations [4,23,31]

$$\frac{1}{J} = \frac{1}{J_L} + \frac{1}{J_K} = \frac{1}{B\varpi^{1/2}} + \frac{1}{J_K} \quad (1)$$

where $J$ is the measured current density, $J_L$ and $J_K$ are the diffusion limiting and kinetic current densities, respectively. $\omega$ is the angular velocity of the disk ($\omega = 2\pi N$, $N$ is the linear rotation speed). $B$ is Levich slope that is expressed by:

$$B = 0.2nFC_0(D_0)^{2/3}\nu^{-1/6} \quad (2)$$

where $n$ is the overall number of electrons transferred in an oxygen reduction process. Based on Eqs. (1) and (2), the transferred electron number ($n$) and $J_K$ can be obtained from the slope and intercept of the Koutecky–Levich plots, respectively. $F$ is the Faraday constant ($F = 96485$ C $mol^{-1}$), $C_0$ is the bulk concentration of $O_2$ in electrolyte solution ($C_0 = 1.2 \times 10^{-3}$ mol $L^{-1}$), $\nu$ is the kinetic viscosity of the electrolyte ($\nu = 0.01$ $cm^2$ $s^{-1}$ in 0.1 M KOH). $D_0$ is the diffusion coefficient of $O_2$ in 0.1 M KOH ($D_0 = 1.9 \times 10^{-5}$ $cm^2$ $s^{-1}$). A constant value of 0.2 is adopted when the rotating speed is expressed in rpm.

## 3. Results and Discussion

### 3.1. Structure and Composition

Fig. 1A shows the SEM image of the fabricated MCNSs after acidification treatment. As shown, uniformly dispersed MCNSs possess an average diameter of ~100 nm. The acidification treatment leads to the formation of rich O-containing hydrophilic surface functional groups (*e.g.*, —COOH, —OH) as confirmed by the FT-IR spectra of MCNSs (Fig. 1B), thus transforming the as-synthesized hydrophobic MCNSs into water dispersible hydrophilic MCNSs (photos (1) and (2), Scheme 1). Such O-rich hydrophilic surface could facilitate the interactions between N-CNDs and MCNSs, favourable for immobilizing N-CNDs onto MCNSs [23,24]. The $N_2$ adsorption–desorption isotherm of the obtained carbon nanospheres after acidification treatment reveals an adsorption–desorption behaviour of type-I curve with a steeply increased adsorption at very low relative pressure, indicating the existence of substantial micropore structures with a pore size

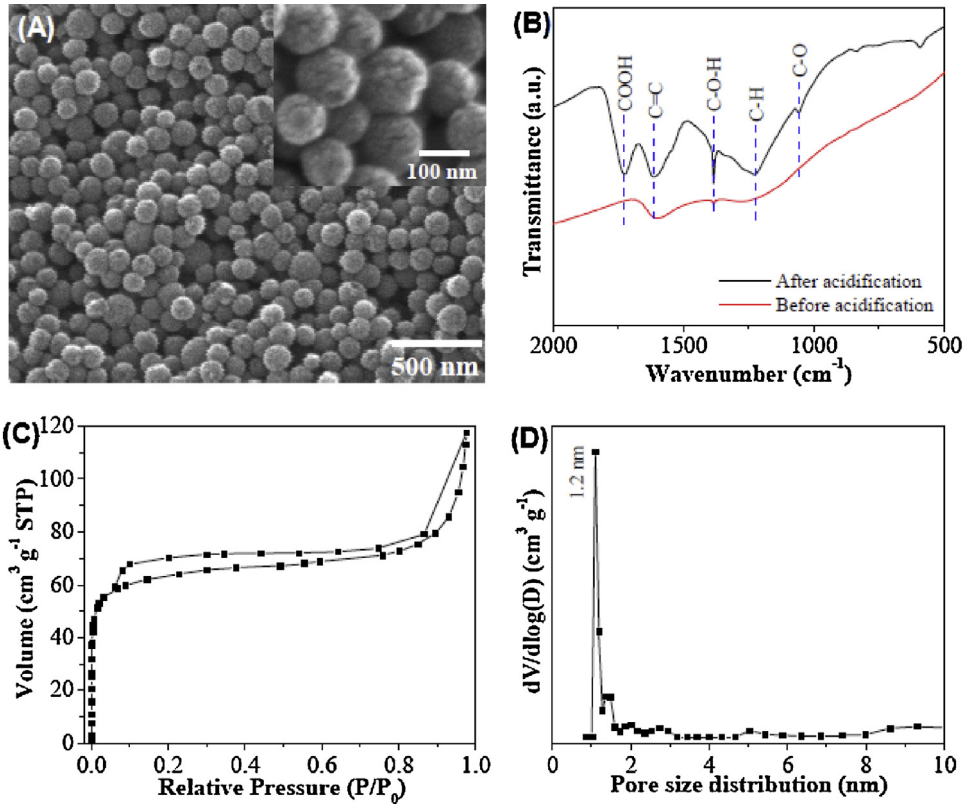


**Fig. 1.** (A) SEM image of MCNSs after acidification treatment. (B) FT-IR spectra of MCNSs before and after acidification treatment. (C) $N_2$ adsorption–desorption isotherm of MCNSs after acidification treatment. (D) Pore size distribution of MCNSs after acidification treatment.

centred at *ca.* 1.2 nm being the predominant ones (Fig. 1C and D) [32]. On basis of the measured adsorption–desorption isotherm, the surface area of MCNSs after acidification was calculated to be *ca.* 241 $m^2 g^{-1}$. The large surface area of MCNSs may be favourable for improving the loading amount of N-CNDs onto MCNSs.

Fig. 2A shows the SEM image of the as-synthesized N-CNDs@MCNSs fabricated by hydrothermal treatment. It can be seen that the carbon nanospheres are connected each other by carbon nanodots, which is obviously different from the acidified MCNSs sample with apparently individual sphere structure (Fig. 1A). To confirm the loading of N-CNDs onto MCNSs, surface element composition of MCNSs before and after hydrothermal treatment with N-CNDs solution was further investigated by XPS technique. The XPS survey spectra of MCNSs and N-CNDs@MCNSs confirm N-CNDs are loaded on the MCNSs after hydrothermal treatment owing to the existence of nitrogen element for N-CNDs@MCNSs (Fig. 2B) [24,29]. The high resolution C 1s and N 1s XPS spectra (Fig. 2C, D) indicate the existence of surface functional groups such as C—C, C—N, C—O, C=O/C=N, C—N—C, $N—(C)_3$, and N—H introduced by the loading of N-CNDs [24,28,29]. The presence of O-containing surface functional groups facilitates the formation of N-CNDs@MCNSs and is favourable for the preparation of stable and uniform N-CNDs@MCNSs catalyst film on glassy carbon electrode [23,24].

### 3.2. Electrocatalytic Performance

The ORR electrocatalytic activity of N-CNDs@MCNSs as electrocatalyst was subsequently evaluated. To obtain meaningful comparison, the measurements of bare glassy carbon (GC), MCNSs coated GC and Pt/C coated GC electrodes are also conducted under identical experimental conditions. Fig. 3A and B show the cyclic voltammetric (CV) responses of bare GC and MCNSs coated GC electrodes in $N_2$ or $O_2$ saturated 0.1 M KOH solutions. As shown, the cathodic current peaks at −0.44 V and −0.39 V can be clearly observed from the CV curves of bare GC electrode and MCNSs coated GC electrode, respectively, which are the characteristics of a typical two-electron transfer ORR process [19,33]. In strong contrast, a dramatically enhanced cathodic current peak at −0.24 V can be observed from a N-CNDs@MCNSs coated GC electrode in $O_2$-saturated 0.1 M KOH solution (Fig. 3C), comparable to the commercial Pt/C electrocatalyst with a cathodic current peak at −0.18 V (Fig. 3D), signifying a four-electron transfer ORR process. Although Pt/C-based materials have been the most effective ORR electrocatalysts, they generally suffer from the cross-over effects of fuel molecules (*e.g.*, methanol) (Fig. 3D) [34]. In this regard, the N-CNDs@MCNSs electrocatalyst displays a high tolerance to methanol cross-over effect (Fig. 3C). From this point, the fabricated N-CNDs@MCNSs is better than the commercial Pt/C electrocatalyst. It should be noted that we also performed ORR measurements using sole N-CNDs as electrocatalyst for meaningful comparison in this work. However, the fabricated N-CNDs catalyst film onto GC electrode is not stable during ORR measurement owing to the high water dispersion property of N-CNDs in alkaline solution, thus resulting in failed ORR measurement. This phenomenon has also been found in our previous report [24]. The above results indicate that the ORR catalytic activity of the nanocomposite could be mainly attributed to N-CNDs, while MCNSs acts as catalyst support to improve the stability of catalyst film onto GC electrode in alkaline solution during ORR measurements.

Fig. 4A shows the linear sweep voltammetric (LSV) responses of bare GC electrode, and MCNSs, N-CNDs@MCNSs and Pt/C coated GC electrodes in $O_2$-saturated 0.1 M KOH solutions under a rotation rate of 1000 rpm with a sweep rate of 5 mV $s^{-1}$. Apparently, the bare GC and MCNSs coated GC electrodes exhibit distinctive characteristics of a two-electron transfer ORR process with the

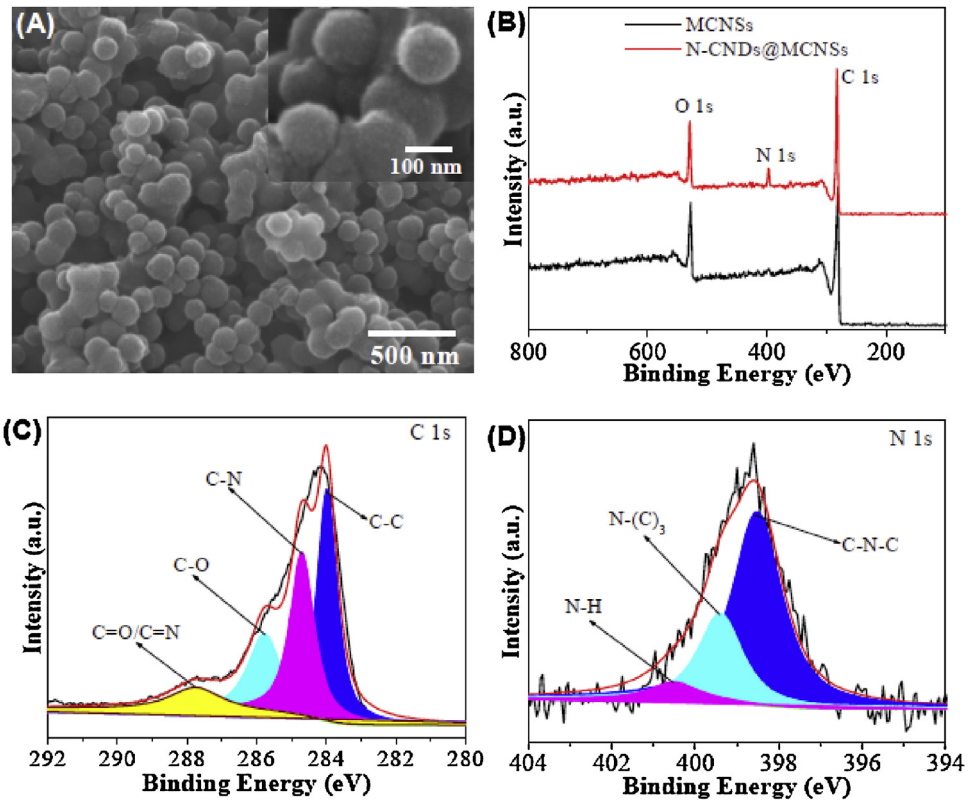


**Fig. 2.** (A) SEM image of N-CNDs coated MCNSs sample fabricated by hydrothermal treatment. (B) Surface survey XPS spectra of MCNSs and N-CNDs@MCNSs. (C) and (D) High resolution C 1s and N 1s XPS spectra of N-CNDs@MCNSs.

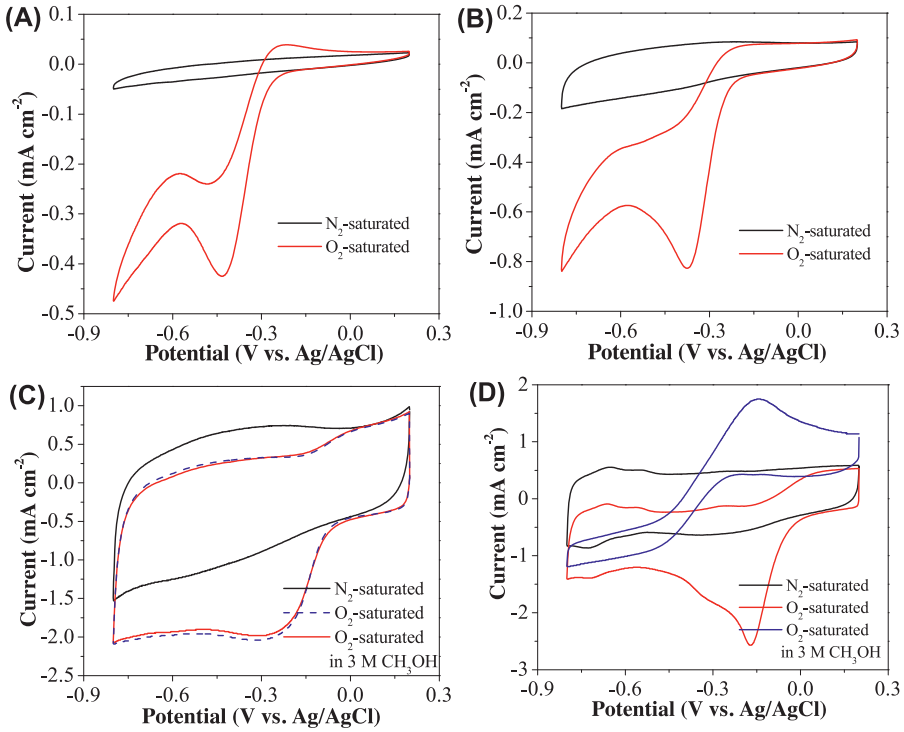


**Fig. 3.** CV responses of bare glassy carbon electrode (A), MCNSs coated glassy carbon electrode (B), N-CNDs@MCNSs coated glassy carbon electrode (C) and commercial Pt/C coated glassy carbon electrode (D) in $N_2$- and $O_2$-saturated 0.1 M KOH solutions with and without 3 M methanol. Scan rate of 100 mV $s^{-1}$.

onset potentials of −0.30 V and −0.26 V, respectively [19,33]. An onset potential of −0.08 V obtained from the N-CNDs/MCNSs coated GC electrode very closes to that obtained from the Pt/C coated GC electrode (onset potential of −0.05 V), indicating an intrinsic low overpotential of N-CNDs@MCNSs for ORR application. Moreover, a wide cathodic current plateau observed from the N-CNDs@MCNSs coated GC electrode within a wide potential range is similar to that observed from the Pt/C electrocatalyst, which is highly desirable for a high efficiency ORR electrocatalyst [20]. Moreover, a superior ORR electrocatalytic activity of the

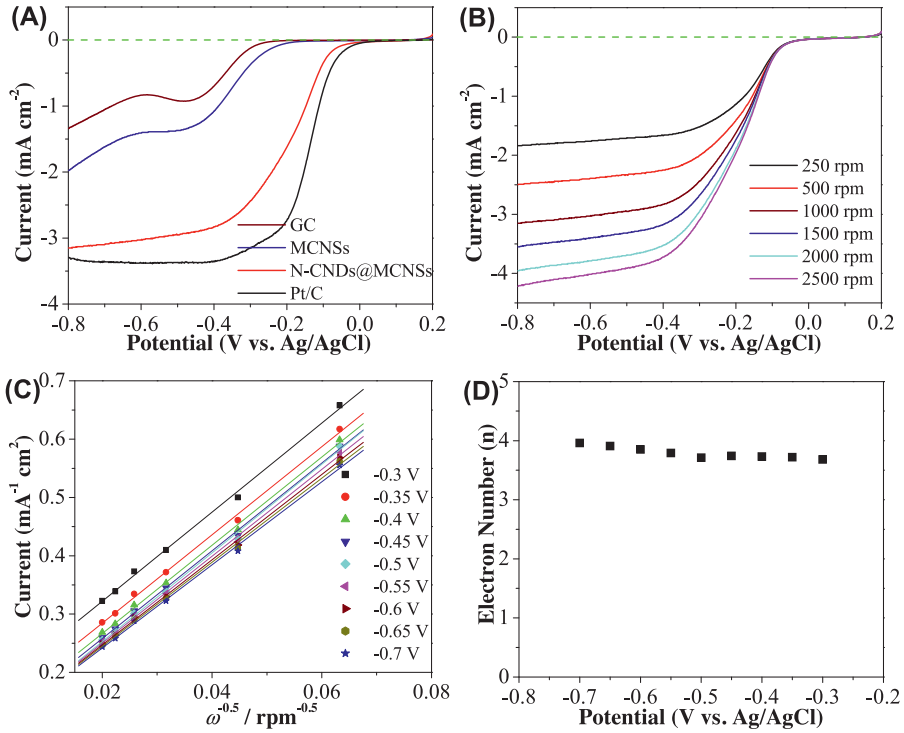


**Fig. 4.** (A) LSV responses of GC, MCNSs, N-CNDs@MCNSs and Pt/C coated GC electrodes at 1000 rpm with a sweep rate of 5 mV $s^{-1}$. (B) LSV curves of N-CNDs@MCNSs at different rotation rates. (C) Koutecky–Levich (K–L) plots derived from the RDE measurements for N-CNDs@MCNSs with different rotation rates. (D) Calculated electron transfer number of N-CNDs@MCNSs.

N-CNDs@MCNSs catalyst can be confirmed by the observed comparable cathodic current density to the commercial Pt/C electrocatalyst (Fig. 4A). It is well known that the transferred electron number in an ORR process is an important parameter to determine the efficiency of an electrocatalyst [4,34]. Fig. 4B shows the LSV responses of the N-CNDs@MCNSs coated GC electrode in an $O_2$-saturated 0.1 M KOH solution under different rotation rates with a sweep rate of 5 mV $s^{-1}$. As shown, the cathodic current density increases with an increase in the rotation rate (from 250 rpm to 2500 rpm). Fig. 4C shows the Koutecky–Levich (K–L) curves measured at different potentials (derived from Fig. 4B). For a given potential, the measured current densities are directly proportional to the square root of the rotation rates for all cases investigated. Such linear relationships indicate a first-order reaction with respect to the dissolved $O_2$ concentration. The transferred electron number ($n$) per $O_2$ molecule for the N-CNDs@MCNSs electrocatalyst calculated from Fig. 4C is found to be between 3.68 and 3.95 within the potential range of −0.3 V to −0.7 V (Fig. 4D), implying a four-electron ORR process [23,24]. The obtained results are comparable to the recent reported results using N-doped carbon nanodot-based composite electrocatalysts [23,24]. However, this obtained ORR performance in this work is obviously better than that obtained by using sole N-doped carbon nanodot electrocatalyst fabricated from soy milk [22].

The operational stability test for long-term use indicates that the N-CNDs@MCNSs coated electrode can maintain over 90% of its original catalytic activity after 5 h of continuous operation under a rotation rate of 1000 rpm and an applied potential of −0.3 V (Fig. 5). However, for the Pt/C coated GC electrode tested under identical conditions, only 76% of its original catalytic activity can be maintained (Fig. 5). This suggests that the N-CNDs@MCNSs coated GC electrode possesses a better operational stability than that of Pt/C electrocatalyst. The superior ORR catalytic performance of the N-CNDs@MCNSs can be attributed to the dual-role of N-CNDs played in the N-CNDs@MCNSs. The N-CNDs introduce electrocatalytic active sites to enhance the electrocatalytic activity owing to N doping [4,24], and join MCNSs together to enhance the stability of catalyst film onto GC electrode. In addition, the formation of N-CNDs@MCNSs also provides effective electron pathways. The electrochemical impedance spectra (EIS) show that the resistance including series resistance and charge transfer resistance of the N-CNDs/MCNSs is comparable to the Pt/C electrocatalyst, but significantly lower than that of MCNSs (Fig. 6), indicating good conductivity and superior electrocatalytic activity of the fabricated N-CNDs@MCNSs as electrocatalyst [35].

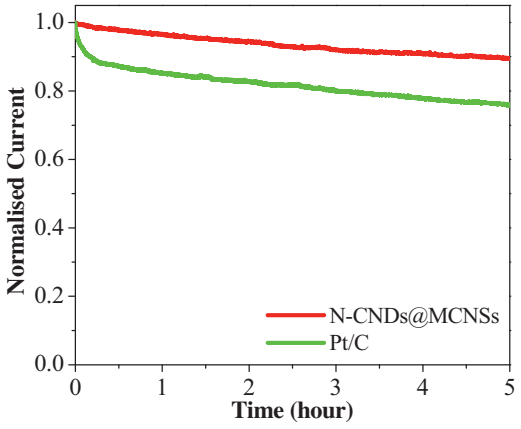


**Fig. 5.** Current-time curves of N-CNDs@MCNSs and Pt/C coated glassy carbon electrodes in $O_2$-saturated 0.1 M KOH solutions with a rotation rate of 1000 rpm at an applied potential of −0.3 V.

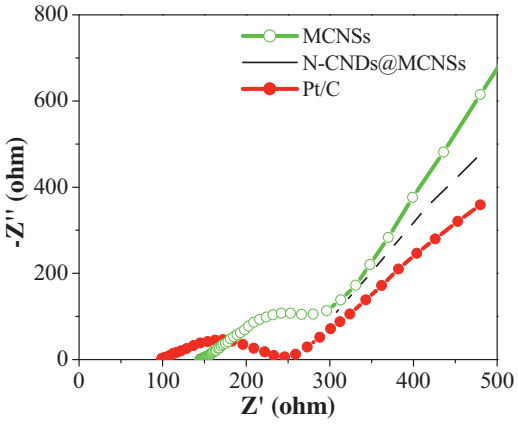


**Fig. 6.** Electrochemical impedance spectra of MCNSs, N-CNDs@MCNSs, and Pt/C coated glassy carbon electrodes in $O_2$-saturated 0.1 M KOH solutions.

The above all advantages contribute high ORR performance of the N-CNDs@MCNSs composite electrocatalyst.

## 4. Conclusions

In summary, we have proposed and experimentally demonstrated a new approach immobilizing N-doped carbon nanodots onto microporous carbon nanospheres *via* a facile hydrothermal process to produce a carbon-based electrocatalyst with superior ORR catalytic activity and operational stability. The findings of this work provide a useful approach to fabricate high performance carbon-based electrocatalysts using cheap and plentiful biomass as carbon sources.

## Acknowledgments

This work was financially supported by Australian Research Council (ARC) Discovery Project and the Natural Science Foundation of China (Grant No. 51372248, 51432009).

## References

[1] A.K. Geim, K.S. Novoselov, The rise of graphene, Nat. Mater. 6 (2007) 183–191.
[2] Z. Cao, B. Wei, A perspective: carbon nanotube macro-films for energy storage, Energy Environ. Sci. 6 (2013) 3183.
[3] X. Yang, C. Cheng, Y. Wang, L. Qiu, D. Li, Liquid-mediated dense integration of graphene materials for compact capacitive energy storage, Science 341 (2013) 534.
[4] K. Gong, F. Du, Z. Xia, M. Durstock, L. Dai, Nitrogen-doped carbon nanotube arrays with high electrocatalytic activity for oxygen reduction, Science 323 (2009) 760.
[5] S.N. Baker, G.A. Baker, Luminescent carbon nanodots: emergent nanolight, Angew. Chem., Int. Ed. 49 (2010) 6726.
[6] G.-w. Cui, W.-l. Wang, M.-y. Ma, M. Zhang, X.-y. Xia, F.-y. Han, X.-f. Shi, Y.-q. Zhao, Y.-B. Dong, B. Tang, Rational design of carbon and $TiO_2$ assembly materials: covered or strewn, which is better for photocatalysis? Chem. Commun. 49 (2013) 6415.
[7] C. Alegre, M.E. Galvez, R. Moliner, V. Baglio, A.S. Arico, M.J. Lazaro, Towards an optimal synthesis route for the preparation of highly mesoporous carbon xerogel-supported Pt catalysts for the oxygen reduction reaction, Appl. Catal., B 147 (2014) 947.
[8] Y. Chen, J. Xu, X. Liu, Y. Tang, T. Lu, Electrostatic self-assembly of platinum nanochains on carbon nanotubes: A highly active electrocatalyst for the oxygen reduction reaction, Appl. Catal. B 140-141 (2013) 552.
[9] C.H. Choi, M.W. Chung, H.C. Kwon, J.H. Chung, S.I. Woo, Nitrogen-doped graphene/carbon nanotube self-assembly for efficient oxygen reduction reaction in acid media, Appl. Catal., B 144 (2014) 760.
[10] M. Yaldagard, N. Seghatoleslami, M. Jahanshahi, Preparation of Pt-Co nanoparticles by galvanostatic pulse electrochemical codeposition on in situ electrochemical reduced graphene nanoplates based carbon paper electrode for oxygen reduction reaction in proton exchange membrane, Appl. Surf. Sci. 315 (2014) 222.
[11] L. Dai, Functionalization of graphene for efficient energy conversion and storage, Acc. Chem. Res. 46 (2013) 31.

[12] J. Yan, H. Zhou, P. Yu, L. Su, L. Mao, Rational functionalization of carbon nanotubes leading to electrochemical devices with striking applications, Adv. Mater. 20 (2008) 2899.
[13] K.T. Al-Jamal, A. Nunes, L. Methven, H. Ali-Boucetta, S. Li, F.M. Toma, M.A. Herrero, W.T. Al-Jamal, H.M.M. ten Eikelder, J. Foster, S. Mather, M. Prato, A. Bianco, K. Kostarelos, Degree of chemical functionalization of carbon nanotubes determines tissue distribution and excretion profile, Angew. Chem., Int. Ed. 51 (2012) 6389.
[14] A. Llanes-Pallas, K. Yoosaf, H. Traboulsi, J. Mohanraj, T. Seldrum, J. Dumont, A. Minoia, R. Lazzaroni, N. Armaroli, D. Bonifazi, Modular engineering of H-bonded supramolecular polymers for reversible functionalization of carbon nanotubes, J. Am. Chem. Soc. 133 (2011) 15412.
[15] Q. Li, S. Zhang, L. Dai, L.-s. Li, Nitrogen-doped colloidal graphene quantum dots and their size-dependent electrocatalytic activity for the oxygen reduction reaction, J. Am. Chem. Soc. 134 (2012) 18932.
[16] S. Wang, L. Zhang, Z. Xia, A. Roy, D.W. Chang, J.-B. Baek, L. Dai, BCN graphene as efficient metal-free electrocatalyst for the oxygen reduction reaction, Angew. Chem., Int. Ed. 51 (2012) 4209.
[17] Y. Li, T. Li, M. Yao, S. Liu, Metal-free nitrogen-doped hollow carbon spheres synthesized by thermal treatment of poly(o-phenylenediamine) for oxygen reduction reaction in direct methanol fuel cell applications, J. Mater. Chem. 22 (2012) 10911.
[18] J. Liang, Y. Jiao, M. Jaroniec, S.Z. Qiao, Sulfur and nitrogen dual-doped mesoporous graphene electrocatalyst for oxygen reduction with synergistically enhanced performance, Angew. Chem., Int. Ed. 51 (2012) 11496.
[19] Z.-W. Liu, F. Peng, H.-J. Wang, H. Yu, W.-X. Zheng, J. Yang, Phosphorus-doped graphite layers with high electrocatalytic activity for the $O_2$ reduction in an alkaline medium, Angew. Chem., Int. Ed. 50 (2011) 3257.
[20] Y. Zheng, Y. Jiao, L. Ge, M. Jaroniec, S.Z. Qiao, Two-step boron and nitrogen doping in graphene for enhanced synergistic catalysis, Angew. Chem., Int. Ed. 52 (2013) 3110.
[21] R. Liu, D. Wu, X. Feng, K. Mullen, Nitrogen-doped ordered mesoporous graphitic arrays with high electrocatalytic activity for oxygen reduction, Angew. Chem., Int. Ed. 49 (2010) 2565.
[22] C. Zhu, J. Zhai, S. Dong, Control the size and surface chemistry of graphene for the rising fluorescent materials, Chem. Commun. 48 (2012) 9367.
[23] Y. Li, Y. Zhao, H. Cheng, Y. Hu, G. Shi, L. Dai, L. Qu, Nitrogen-doped graphene quantum dots with oxygen-rich functional groups, J. Am. Chem. Soc. 134 (2012) 15.
[24] H. Zhang, Y. Wang, D. Wang, Y. Li, X. Liu, P. Liu, H. Yang, T. An, Z. Tang, H. Zhao, Hydrothermal transformation of dried grass into graphitic carbon-based high performance electrocatalyst for oxygen reduction reaction, Small 10 (2014) 3371.
[25] Z.-Y. Shih, A.P. Periasamy, P.-C. Hsu, H.-T. Chang, Synthesis and catalysis of copper sulfide/carbon nanodots for oxygen reduction in direct methanol fuel cells, Appl. Catal. B 132–133 (2013) 363.
[26] M. Liu, W. Chen, Green synthesis of silver nanoclusters supported on carbon nanodots: enhanced photoluminescence and high catalytic activity for oxygen reduction reaction, Nanoscale 5 (2013) 12558.
[27] Y. Fang, D. Gu, Y. Zou, Z. Wu, F. Li, R. Che, Y. Deng, B. Tu, D. Zhao, A low-concentration hydrothermal synthesis of biocompatible ordered mesoporous carbon nanospheres with tunable and uniform size, Angew. Chem., Int. Ed. 49 (2010) 7987.
[28] S. Liu, J. Tian, L. Wang, Y. Zhang, X. Qin, Y. Luo, A.M. Asiri, A.O. Al-Youbi, X. Sun, Hydrothermal treatment of grass: a low-cost, green route to nitrogen-doped, carbon-rich, photoluminescent polymer nanodots as an effective fluorescent sensing platform for label-free detection of Cu(II) ions, Adv. Mater. 24 (2012) 2037.
[29] H. Zhang, Y. Li, X. Liu, P. Liu, Y. Wang, T. An, H. Yang, D. Jing, H. Zhao, Determination of iodide via direct fluorescence quenching at nitrogen-doped carbon quantum dot fluorophores, Environ. Sci. Technol. Lett. 1 (2014) 87.
[30] D. Gong, C.A. Grimes, O.K. Varghese, W. Hu, R.S. Singh, Z. Chen, E.C. Dickey, Titanium oxide nanotube arrays prepared by anodic oxidation, J. Mater. Res. 16 (2001) 3331.
[31] L. Qu, Y. Liu, J.-B. Baek, L. Dai, Nitrogen-doped graphene as efficient metal-free electrocatalyst for oxygen reduction in fuel cells, ACS Nano 4 (2010) 1321.
[32] Z. Jin, H.-Y. Zhao, X.-J. Zhao, Q.-R. Fang, J.R. Long, G.-S. Zhu, A novel microporous MOF with the capability of selective adsorption of xylenes, Chem. Commun. 46 (2010) 8612.
[33] T. Ohsaka, L. Mao, K. Arihara, T. Sotomura, Bifunctional catalytic activity of manganese oxide toward $O_2$ reduction: novel insight into the mechanism of alkaline air electrode, Electrochem. Commun. 6 (2004) 273.
[34] D. Wang, H.L. Xin, R. Hovden, H. Wang, Y. Yu, D.A. Muller, F.J. Di Salvo, H.D. Abruna, Structurally ordered intermetallic platinum-cobalt core-shell nanoparticles with enhanced activity and stability as oxygen reduction electrocatalysts, Nat. Mater. 12 (2013) 81.
[35] J. Duan, Y. Zheng, S. Chen, Y. Tang, M. Jaroniec, S. Qiao, Mesoporous hybrid material composed of $Mn_3O_4$ nanoparticles on nitrogen-doped graphene for highly efficient oxygen reduction reaction, Chem. Commun. 49 (2013) 7705.